Revised Supplementary Material

3-Cyanopyridine as bridging and terminal ligand in coordination polymers

Miriam Heine, Lothar Fink, Martin U. Schmidt*

Institute of Inorganic and Analytical Chemistry, Goethe University, Max-von-Laue-Str. 7, 60438 Frankfurt am Main, Germany. E-Mail: m.schmidt@chemie.uni-frankfurt.de; Fax: +49 69798 29235; Tel: +49 69798 29123

Figures

Tables

Experimental Details

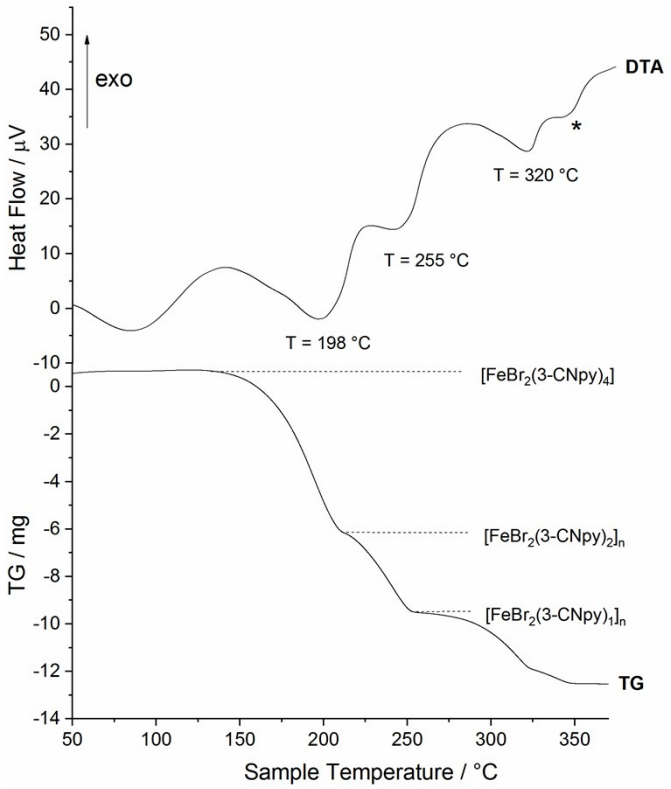

Figure S1. DTA/TG curves of $[FeBr_2(3\text{-}CNpy)_4]$ (**2a**). Heating rate: 5 K/min, Ar atmosphere, Al_2O_3 crucible. The shoulder marked by a * points to a fourth decomposition product $[FeBr_2(3\text{-}CNpy)_{1-x}]_n$, which could not be isolated in the Fe series, but would explain foreign reflections in the XRPD pattern of $[FeBr_2(3\text{-}CNpy)_1]_n$.

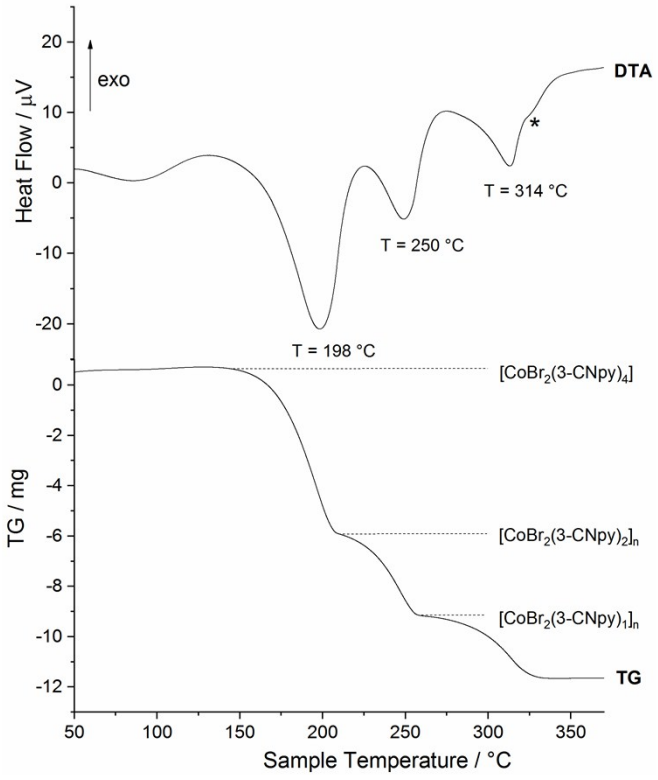

Figure S2. DTA/TG curves of $[CoBr_2(3\text{-}CNpy)_4]$ (**3a**). Heating rate: 5 K/min, Ar atmosphere, Al_2O_3 crucible. The shoulder marked by a * points to a fourth decomposition product $[CoBr_2(3\text{-}CNpy)_{1-x}]_n$, which could not be isolated in the Co series, but would explain foreign reflections in the XRPD pattern of $[CoBr_2(3\text{-}CNpy)_1]_n$.

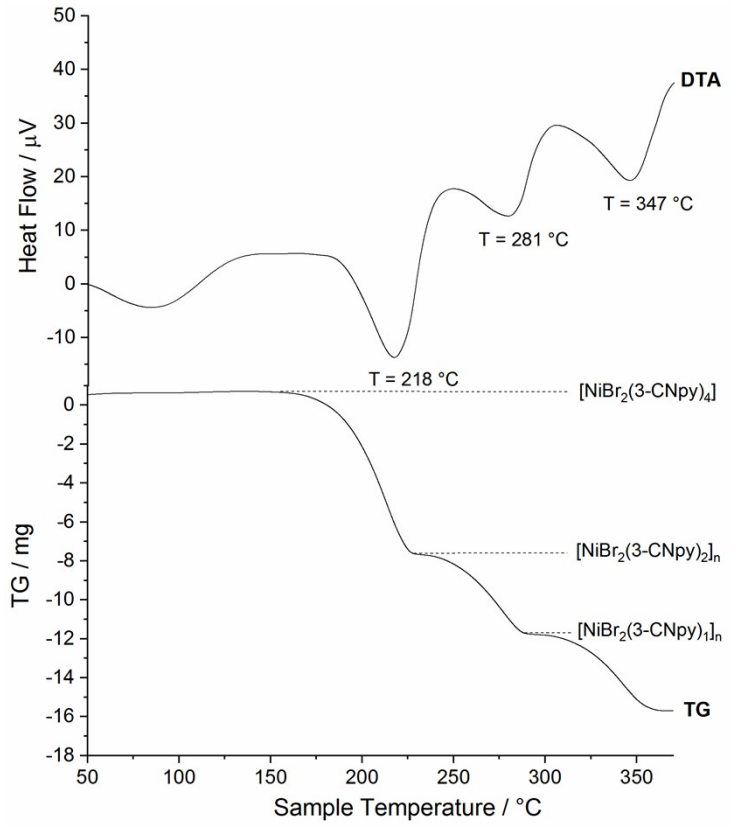

Figure S3. DTA/TG curves of $[NiBr_2(3\text{-}CNpy)_4]$ (**4a**). Heating rate: 5 K/min, Ar atmosphere, Al_2O_3 crucible.

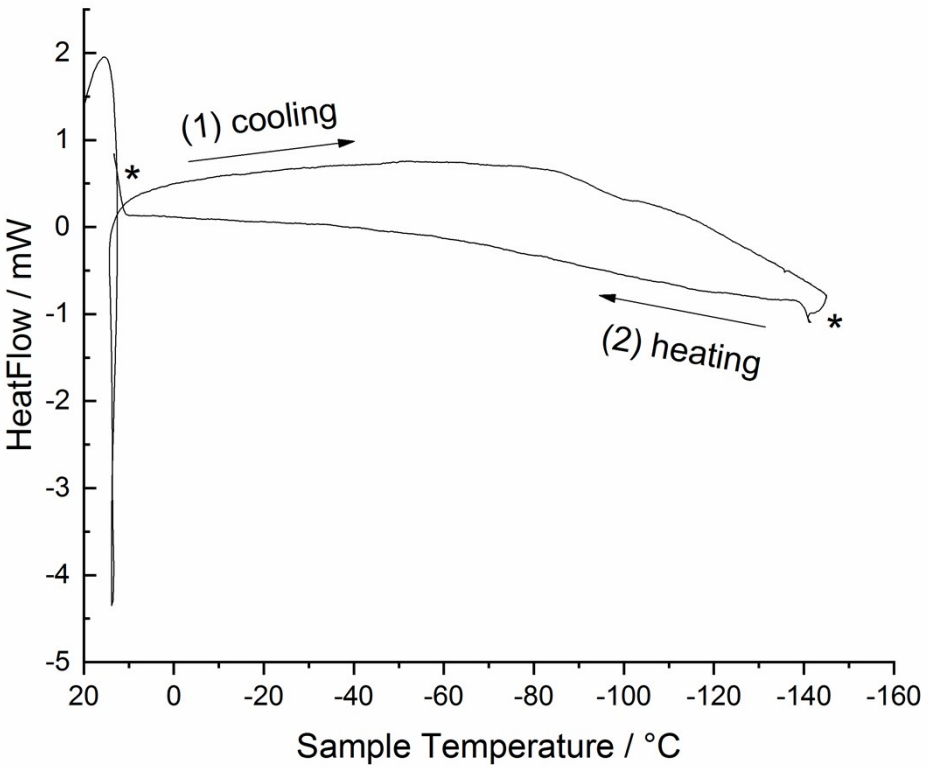

Figure S4. DSC-curve of $[NiBr_2(3\text{-}CNpy)_2]_n$ (**β-4b**). (1) cooling from room temperature to -150°C, then (2) heating to room temperature. Instrumental artefacts are marked by stars.

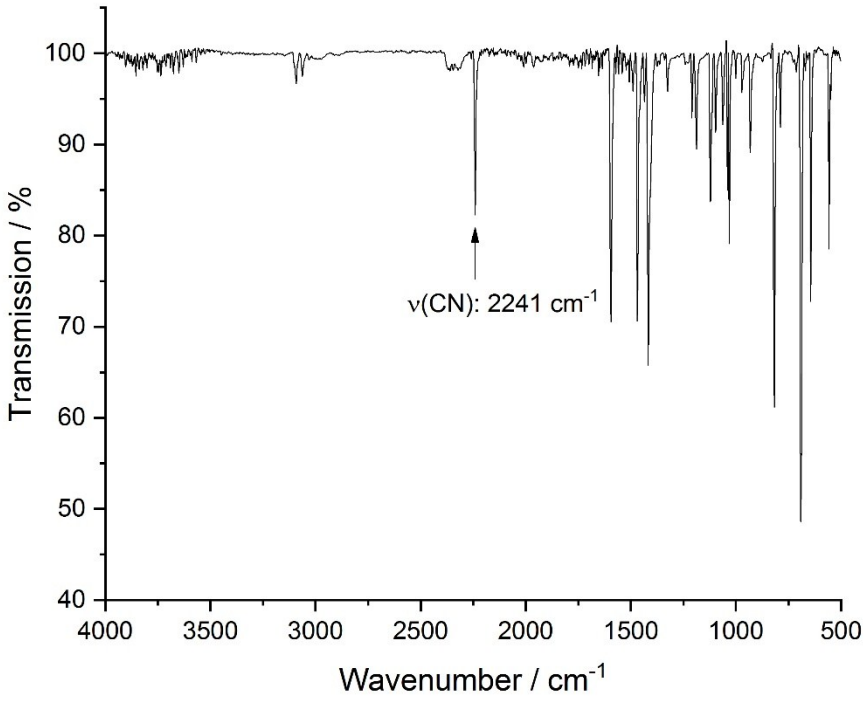

Figure S5. IR spectrum of $[MnBr_2(3\text{-}CNpy)_4]$ (**1a**)

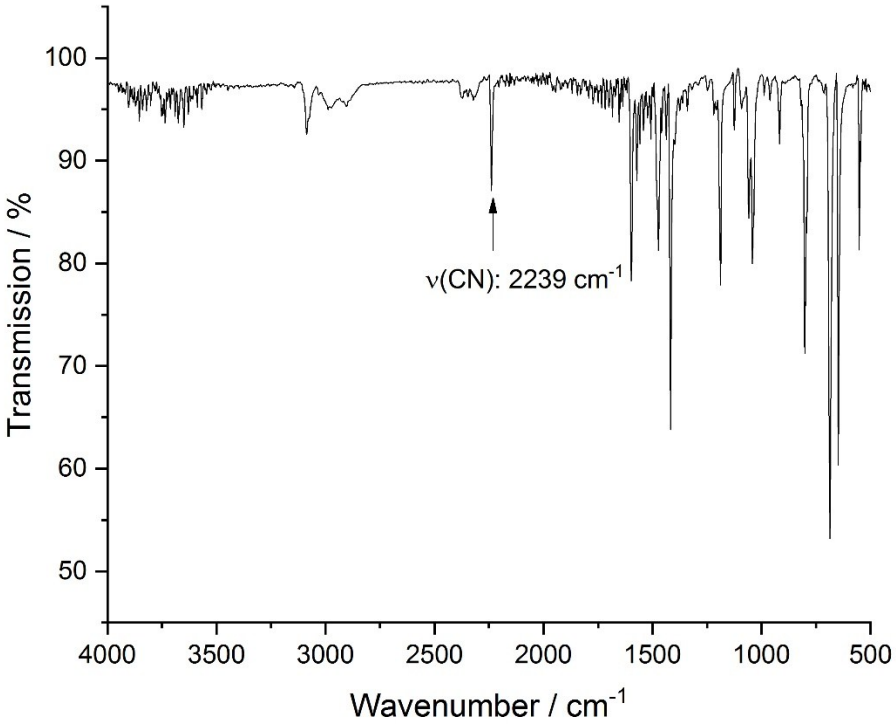

Figure S6. IR spectrum of $[MnBr_2(3\text{-}CNpy)_2]_n$ (**1b**)

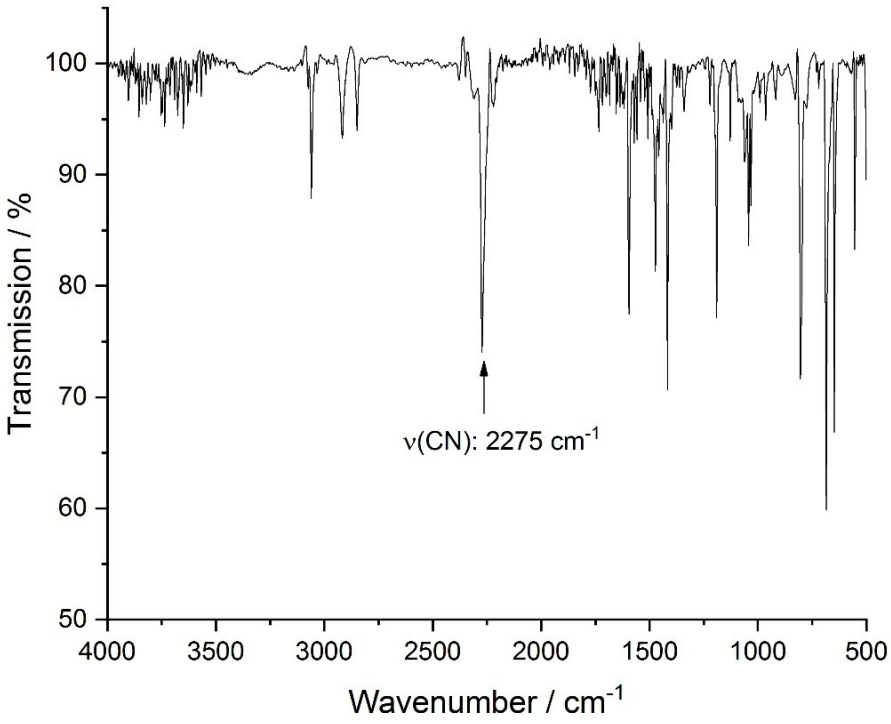

Figure S7. IR spectrum of $[MnBr_2(3\text{-}CNpy)_1]_n$ (**1c**)

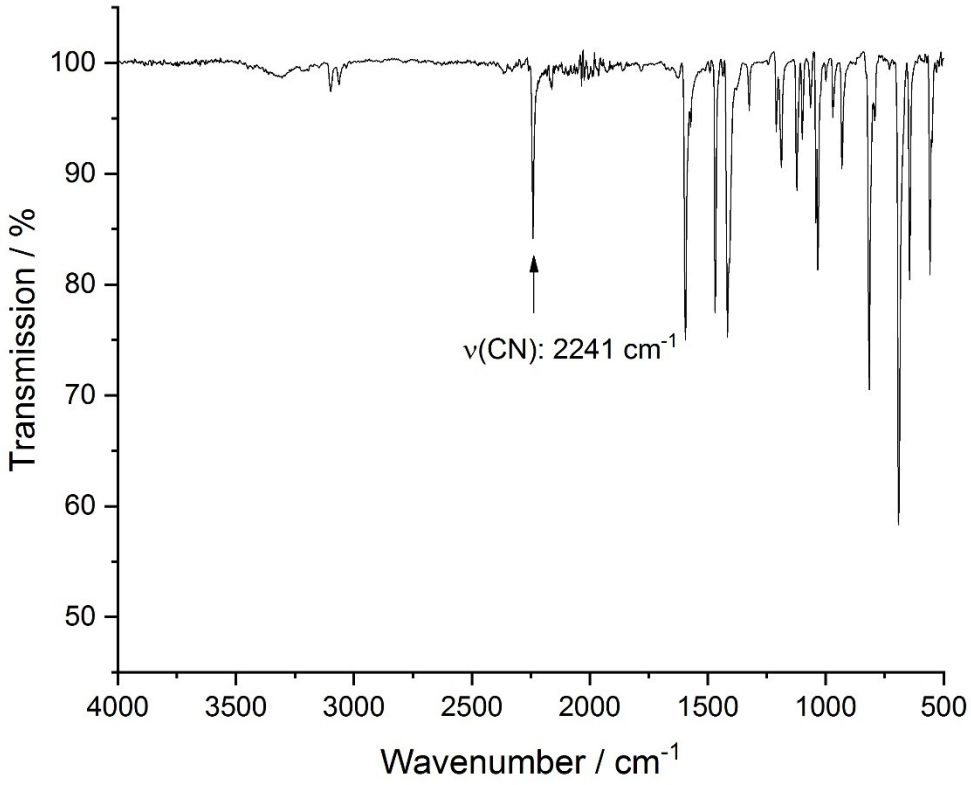

Figure S8. IR spectrum of $[FeBr_2(3\text{-}CNpy)_4]$ (**2a**)

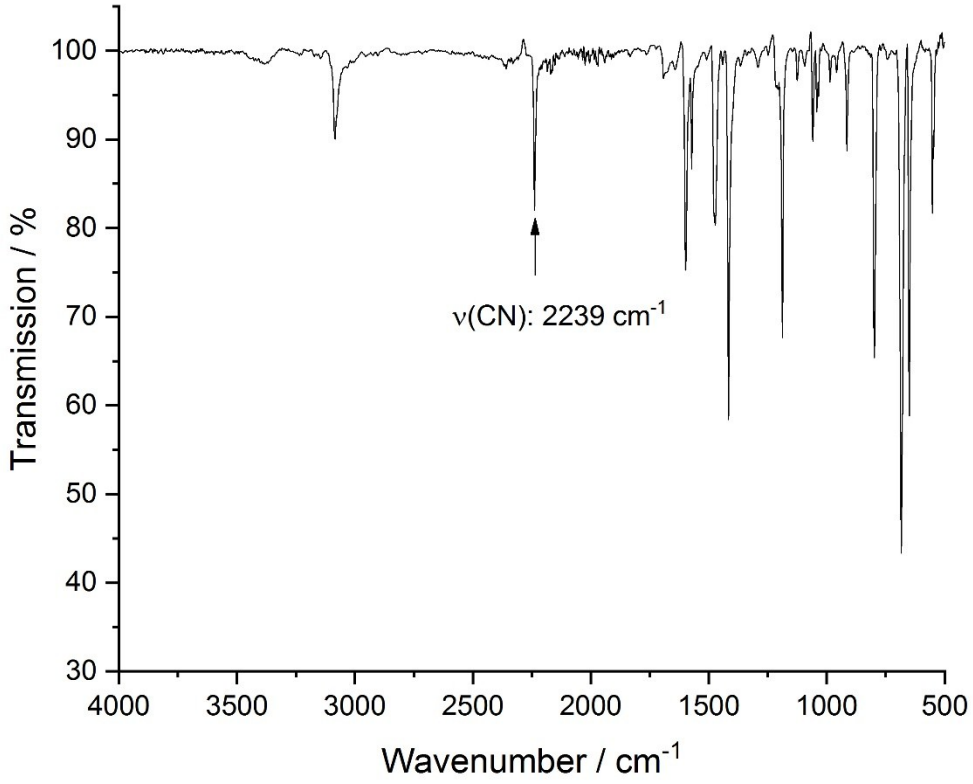

Figure S9. IR spectrum of $[FeBr_2(3\text{-}CNpy)_2]_n$ (**2b**)

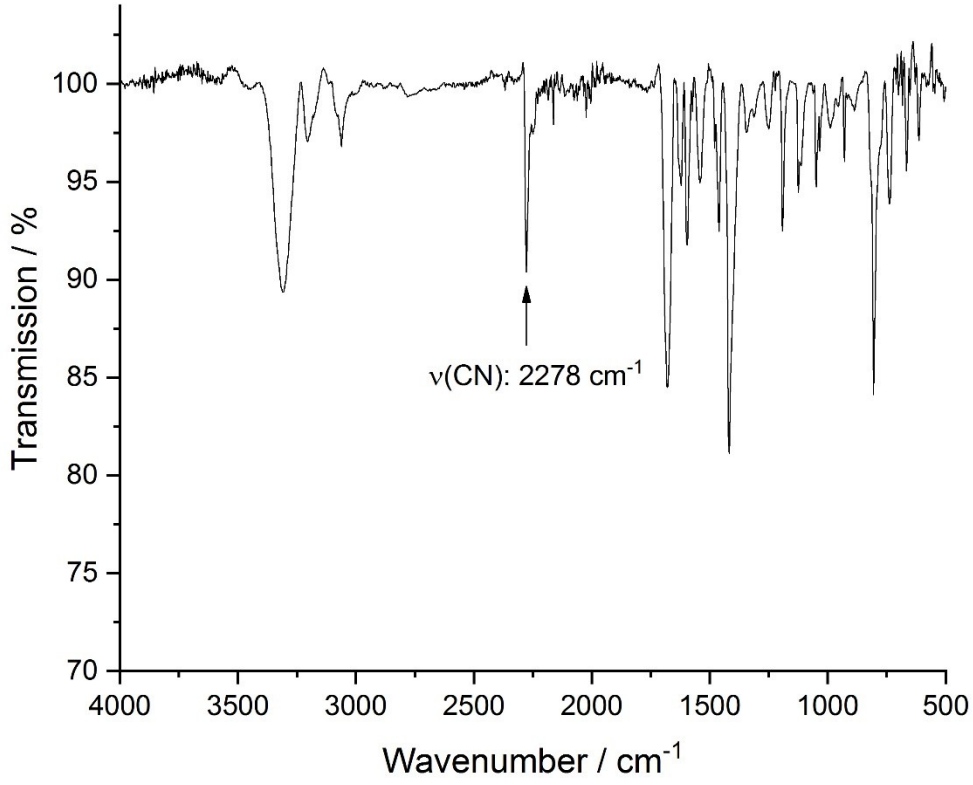

Figure S10. IR spectrum of $[FeBr_2(3\text{-}CNpy)_1]_n$ (**2c**)

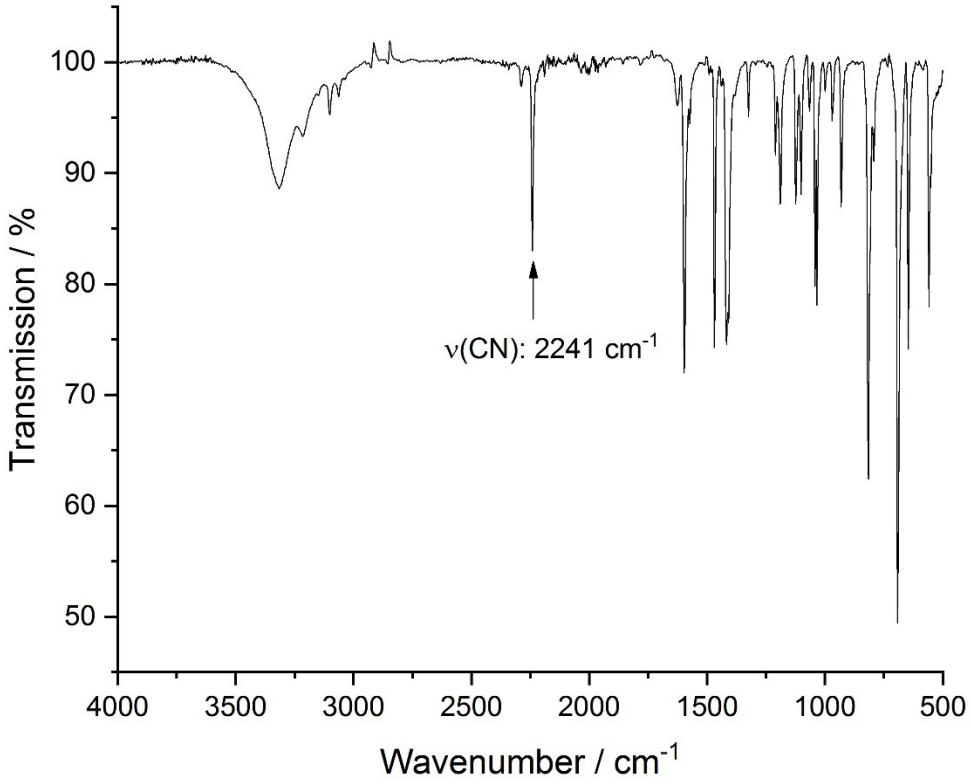

Figure S11. IR spectrum of $[CoBr_2(3\text{-}CNpy)_4]$ (**3a**)

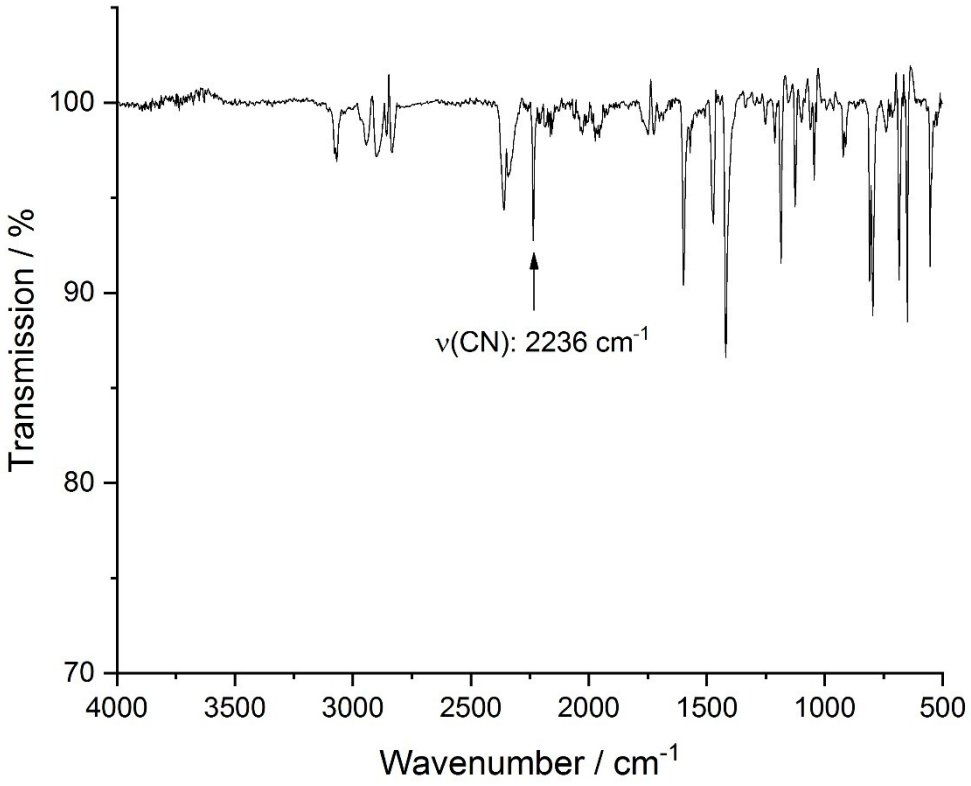

Figure S12. IR spectrum of $[CoBr_2(3\text{-}CNpy)_2]_n$: mixture of **α-3b** and **β-3b**

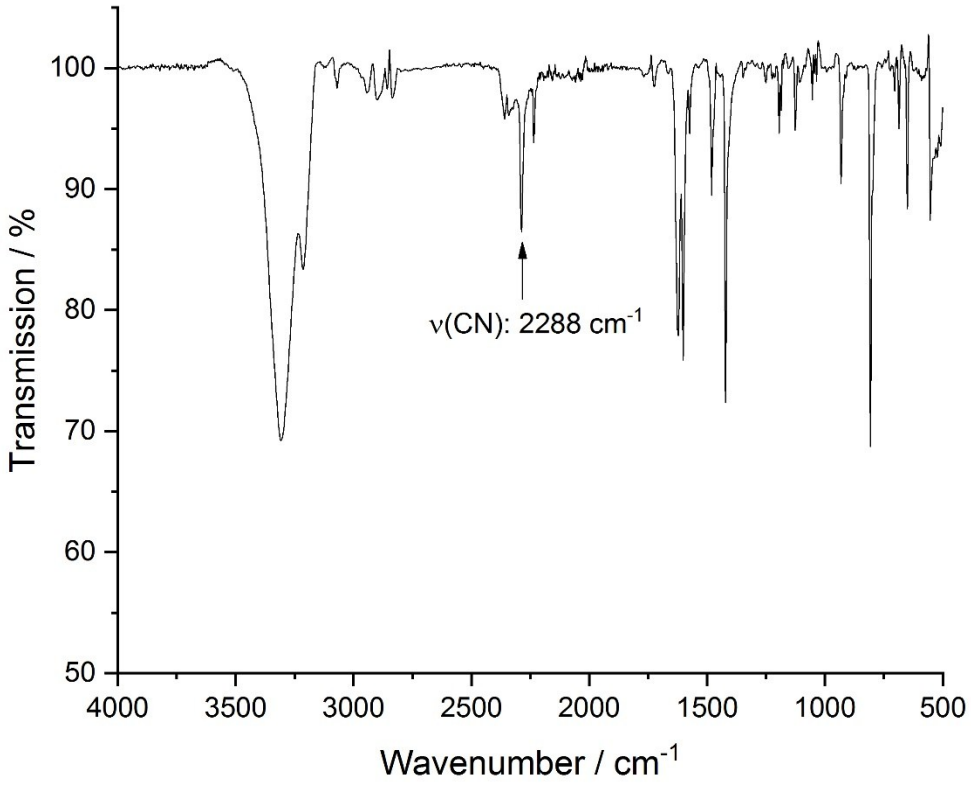

Figure S13. IR spectrum of $[CoBr_2(3\text{-}CNpy)_1]_n$ (**3c**)

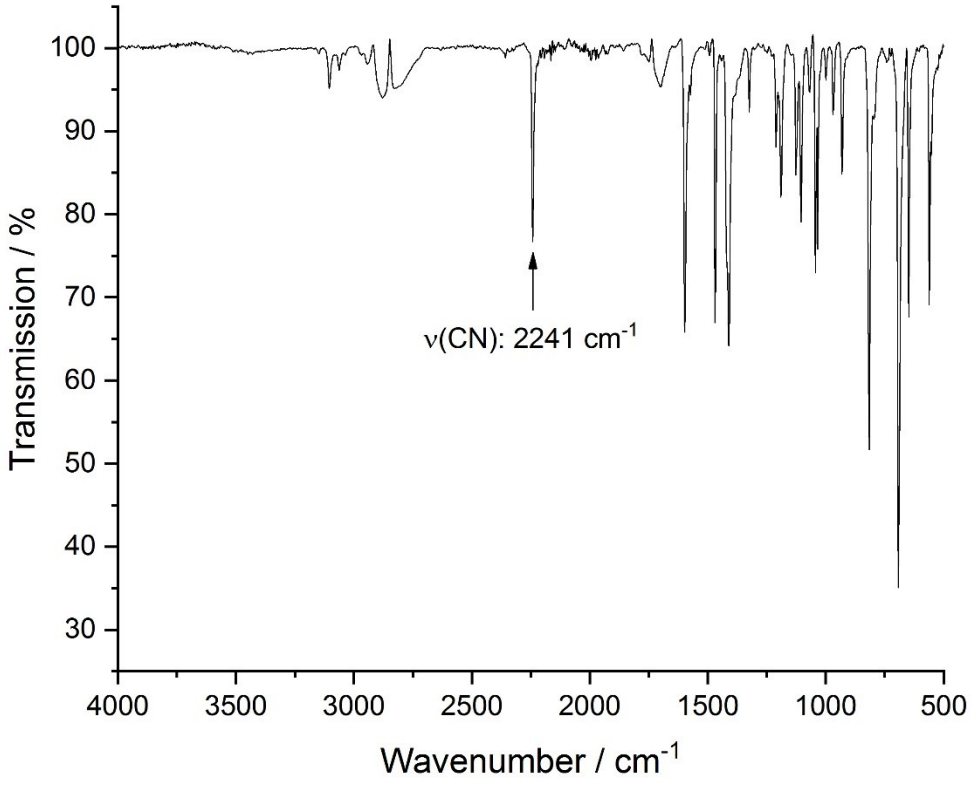

Figure S14. IR spectrum of $[NiBr_2(3\text{-}CNpy)_4]$ (**4a**)

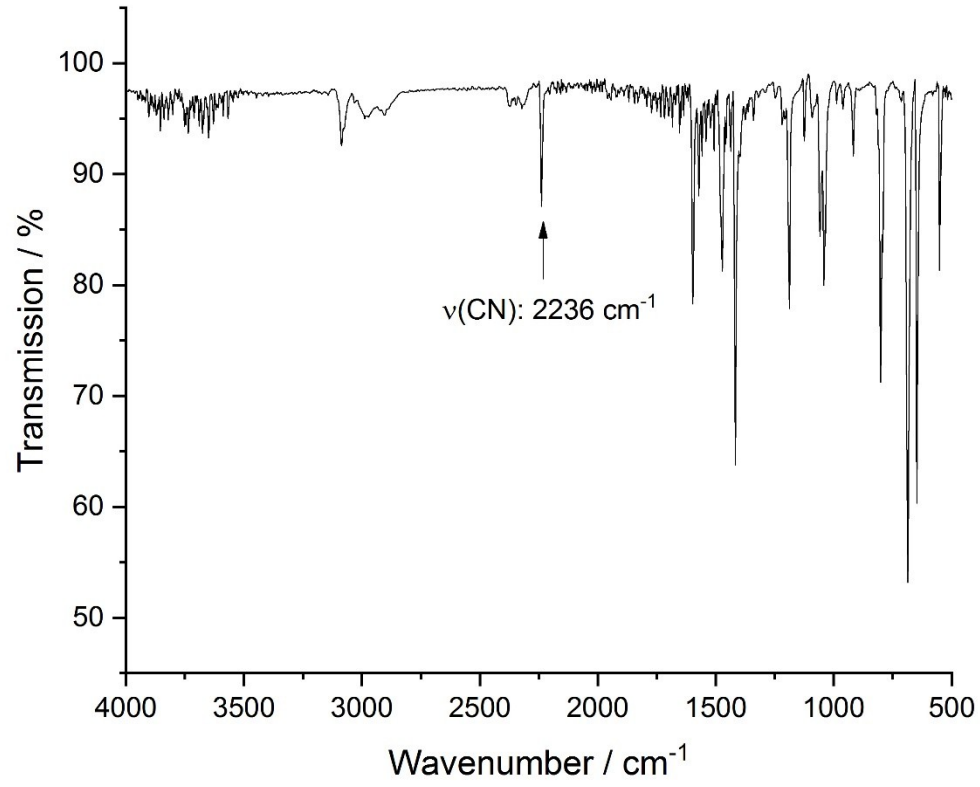

Figure S15. IR spectrum of $[NiBr_2(3\text{-}CNpy)_2]_n$: mixture of **α-4b** and **β-4b**

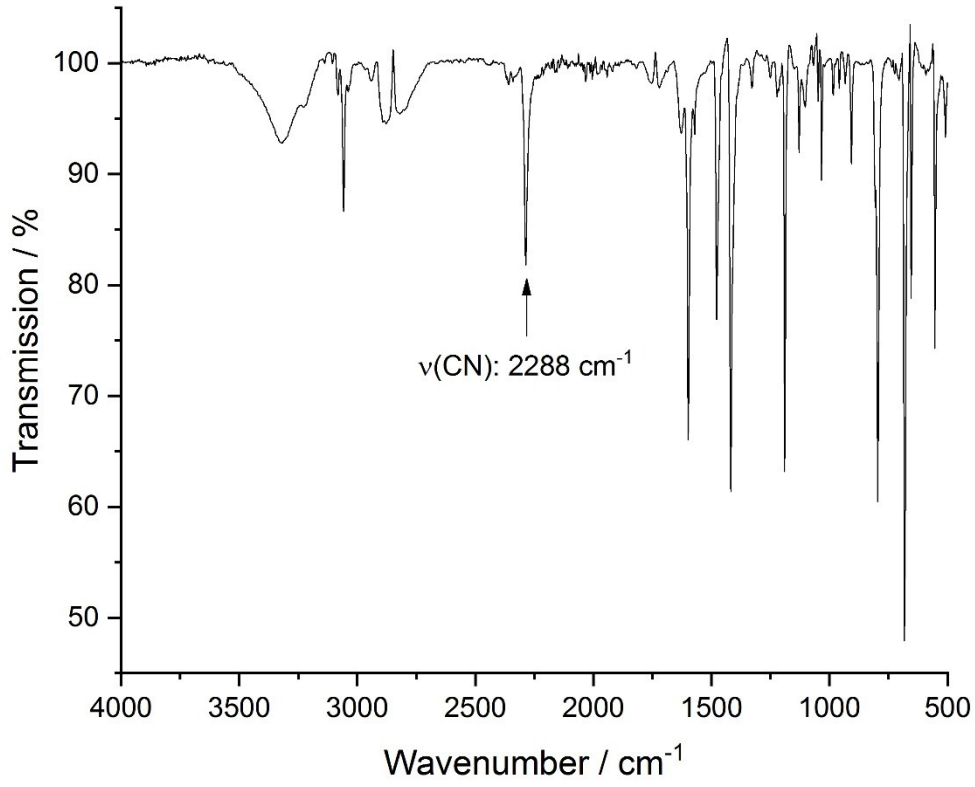

Figure S16. IR spectrum of $[NiBr_2(3\text{-}CNpy)_1]_n$ (**4c**)

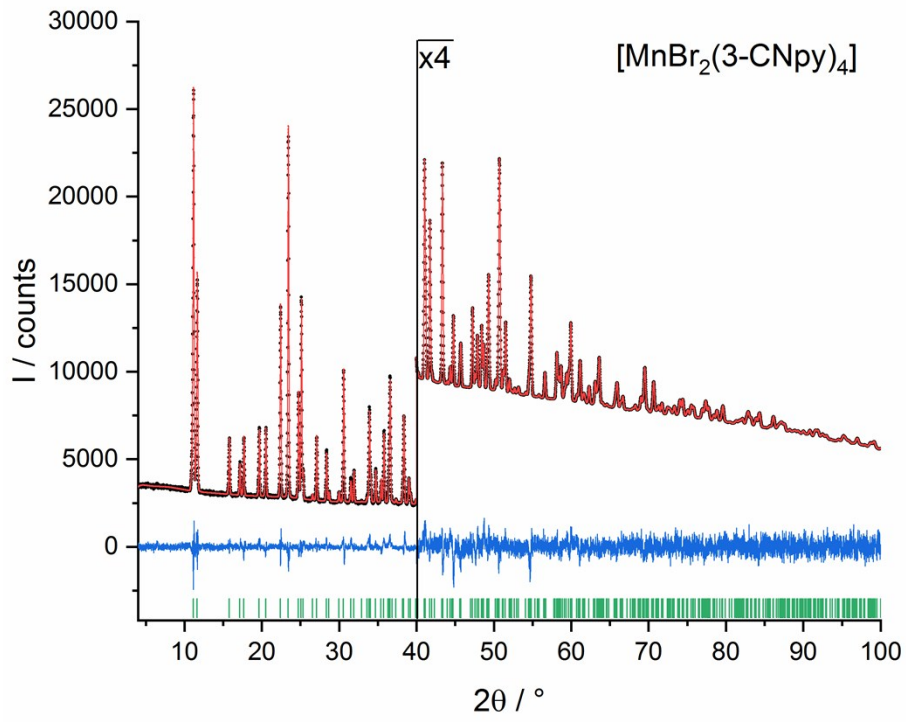

Figure S17. Rietveld plot of **1a**. Observed powder diagram (black points), simulated powder diagram (red solid line), difference profile (blue solid line) and reflection positions (green tick marks). Change of the scale with corresponding factor is indicated in the diagram.

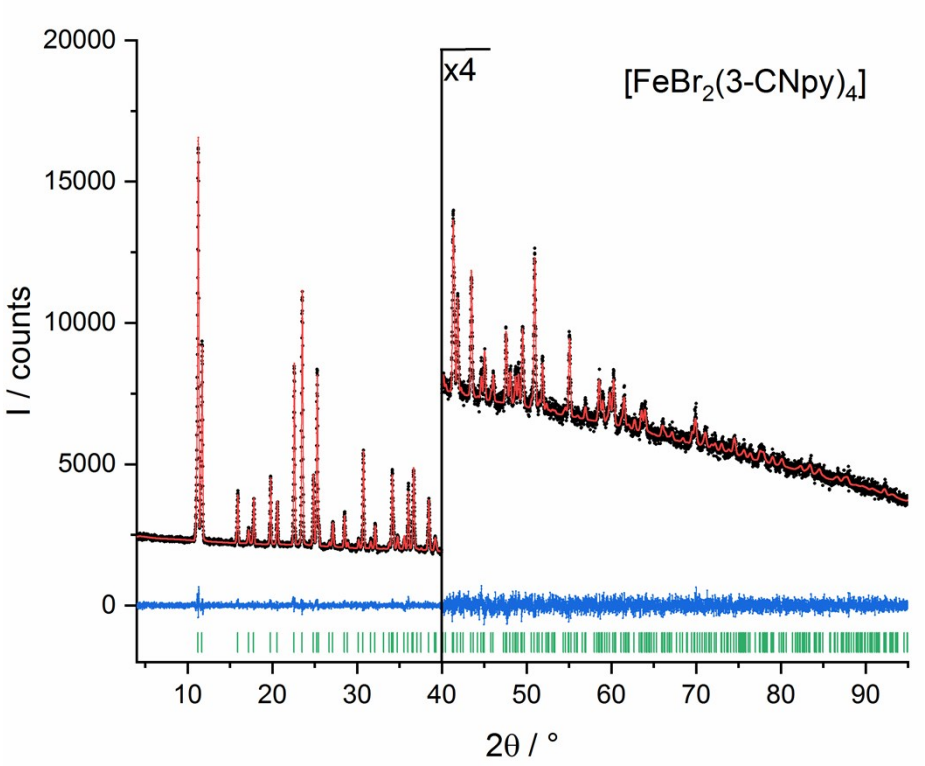

Figure S18. Rietveld plot of **2a**. Observed powder diagram (black points), simulated powder diagram (red solid line), difference profile (blue solid line) and reflection positions (green tick marks). Change of the scale with corresponding factor is indicated in the diagram.

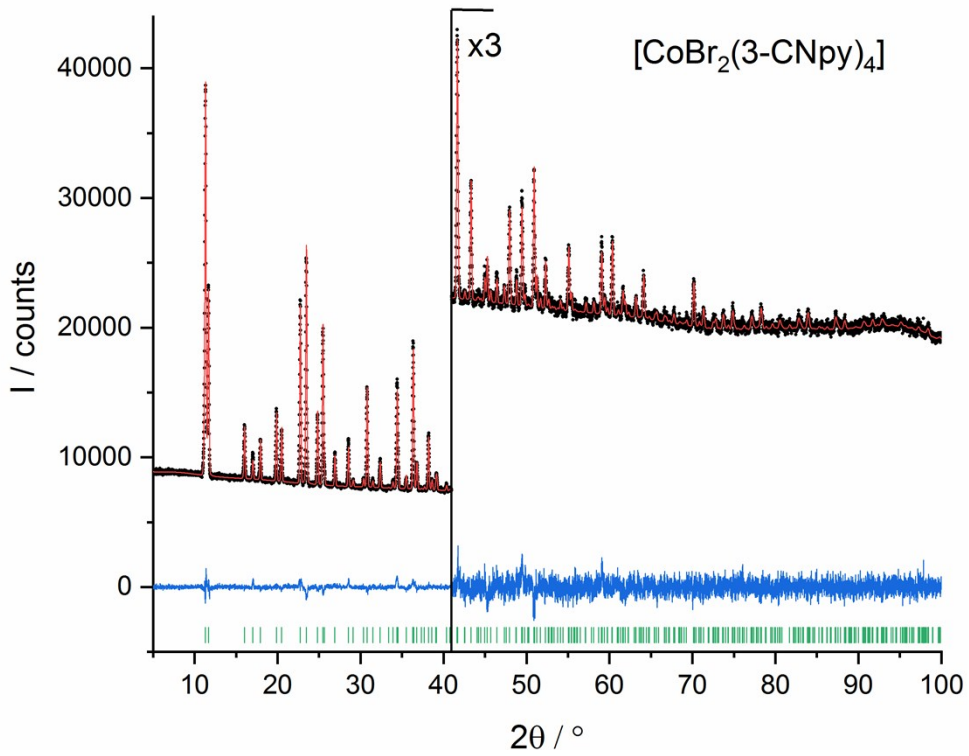

Figure S19. Rietveld plot of **3a**. Observed powder diagram (black points), simulated powder diagram (red solid line), difference profile (blue solid line) and reflection positions (green tick marks). Change of the scale with corresponding factor is indicated in the diagram.

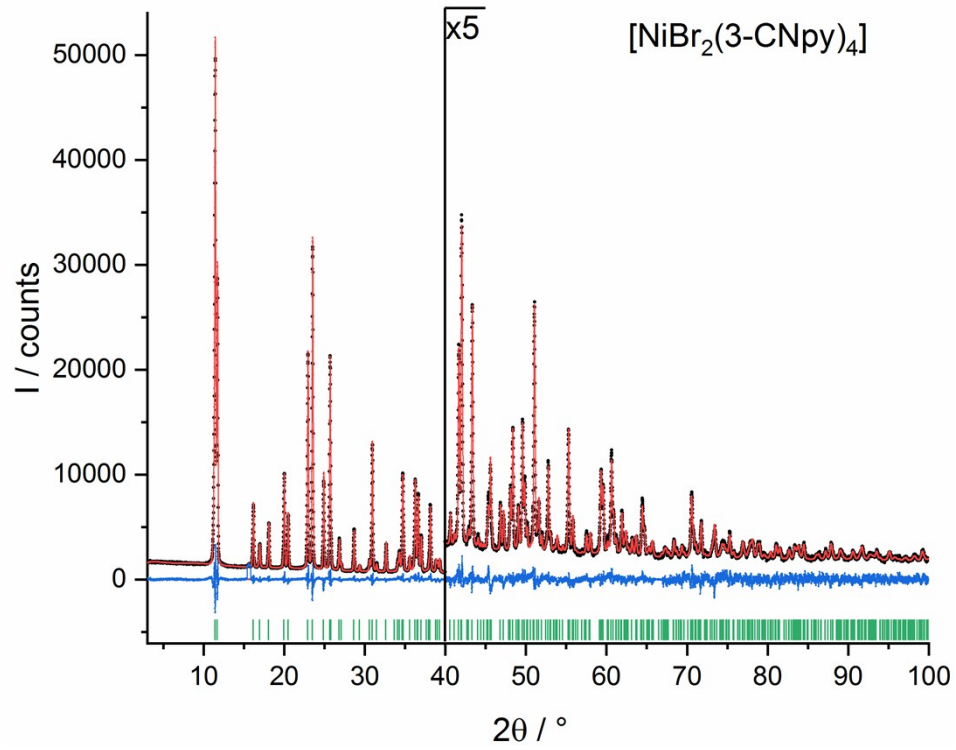

Figure S20. Rietveld plot of **4a**. Observed powder diagram (black points), simulated powder diagram (red solid line), difference profile (blue solid line) and reflection positions (green tick marks). Change of the scale with corresponding factor is indicated in the diagram.

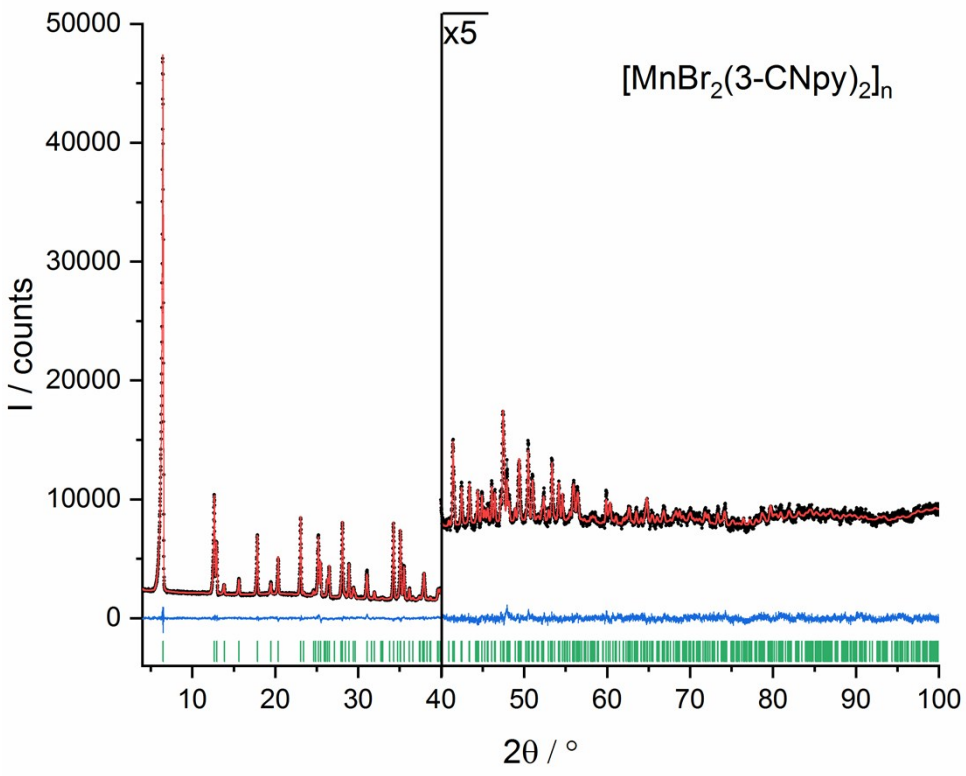

Figure S21. Rietveld plot of **1b**. Observed powder diagram (black points), simulated powder diagram (red solid line), difference profile (blue solid line) and reflection positions (green tick marks). Change of the scale with corresponding factor is indicated in the diagram.

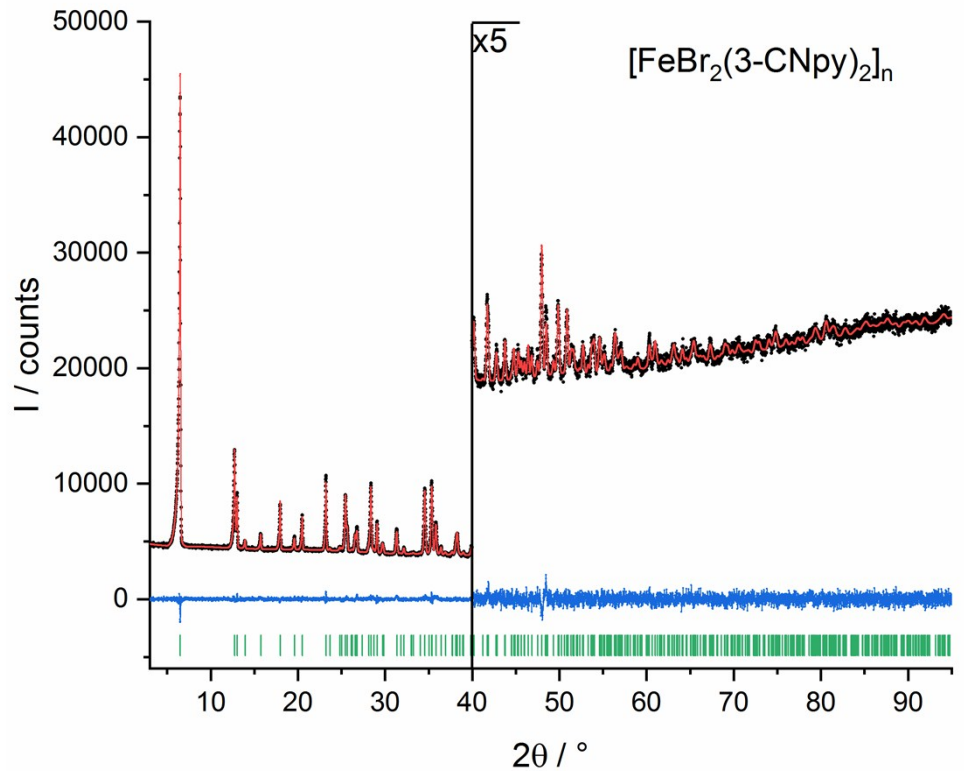

Figure S22. Rietveld plot of **2b**. Observed powder diagram (black points), simulated powder diagram (red solid line), difference profile (blue solid line) and reflection positions (green tick marks). Change of the scale with corresponding factor is indicated in the diagram.

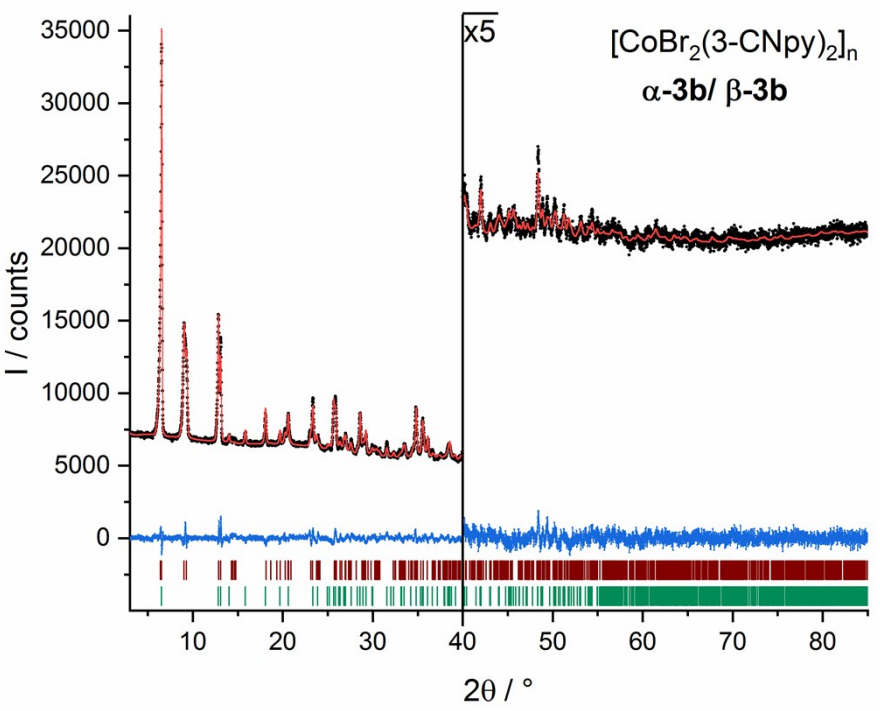

Figure S23. Rietveld plot of **3b**. The crystal structures of **α-3b** and **β-3b** were refined from a phase mixture. Observed powder diagram (black points), simulated powder diagram (red solid line), difference profile (blue solid line) and reflection positions (green tick marks for **α-3b**, brown tick marks for **β-3b**). Change of the scale with corresponding factor is indicated in the diagram.

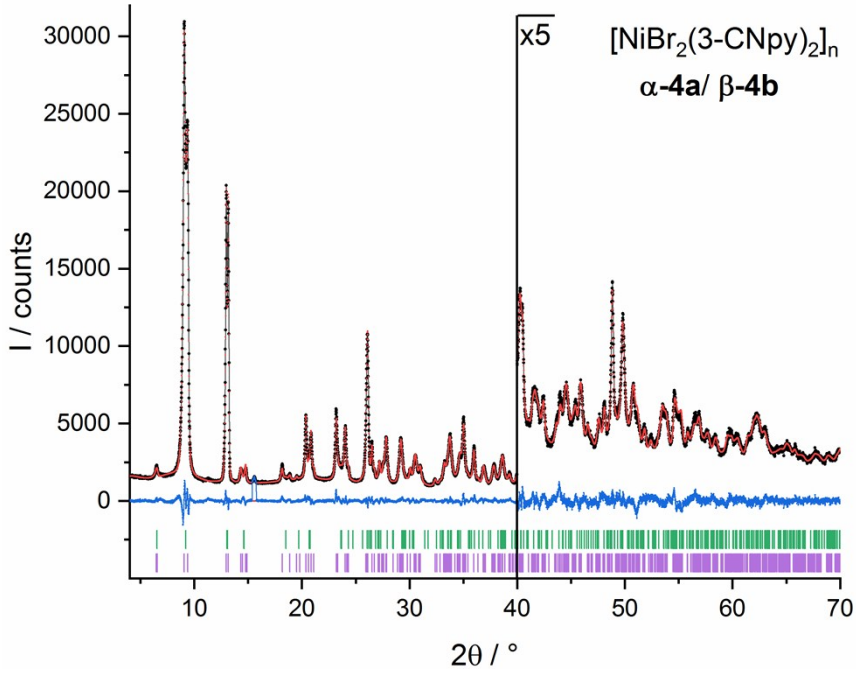

Figure S24. Rietveld plot of **4b**. The crystal structures of **β-4b** was refined from a phase mixture of **α-4b** and **β-4b**. Observed powder diagram (black points), simulated powder diagram (red solid line), difference profile (blue solid line) and reflection positions (green tick marks for **α-4b**, violet tick marks for **β-4b**). Change of the scale with corresponding factor is indicated in the diagram. Excluded region is indicated.

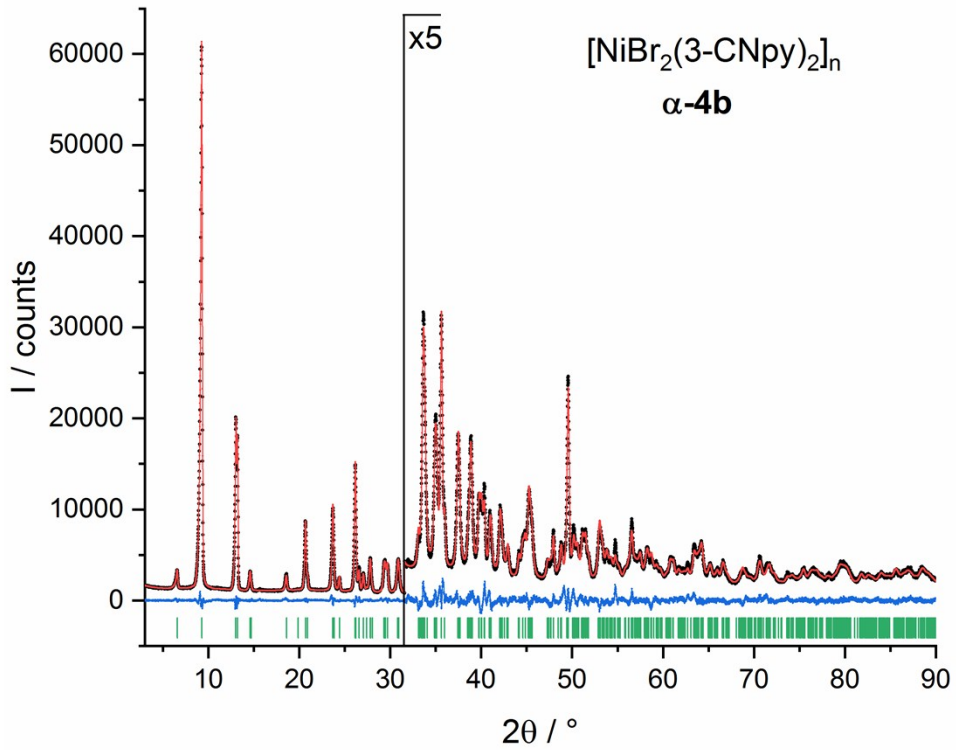

Figure S25. Rietveld plot of **α-4b**. Observed powder diagram (black points), simulated powder diagram (red solid line), difference profile (blue solid line) and reflection positions (green tick marks). Change of the scale with corresponding factor is indicated in the diagram.

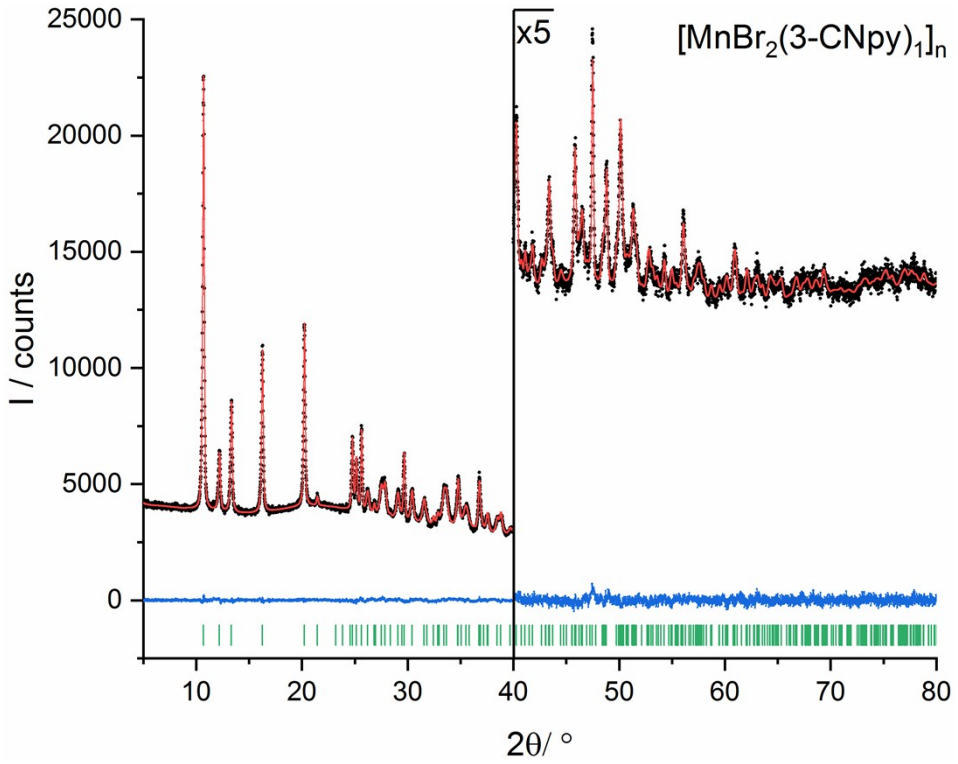

Figure S26. Rietveld plot of **1c**. Observed powder diagram (black points), simulated powder diagram (red solid line), difference profile (blue solid line) and reflection positions (green tick marks). Change of the scale with corresponding factor is indicated in the diagram.

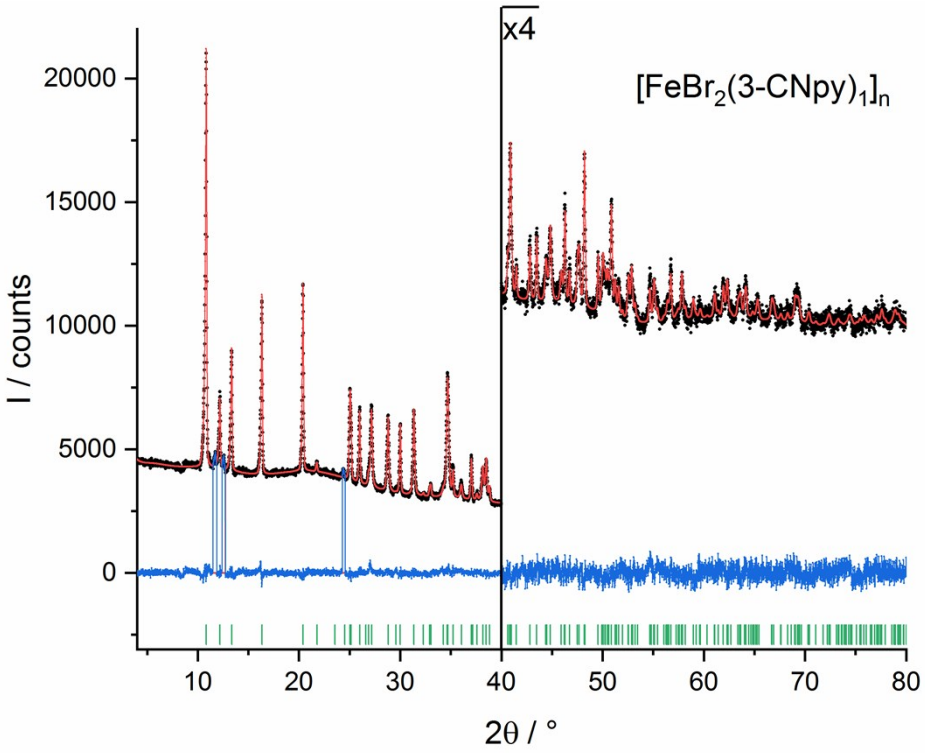

Figure S27. Rietveld plot of **2c**. Observed powder diagram (black points), simulated powder diagram (red solid line), difference profile (blue solid line) and reflection positions (green tick marks). Change of the scale with corresponding factor is indicated in the diagram. Reflections of a foreign phase are excluded.

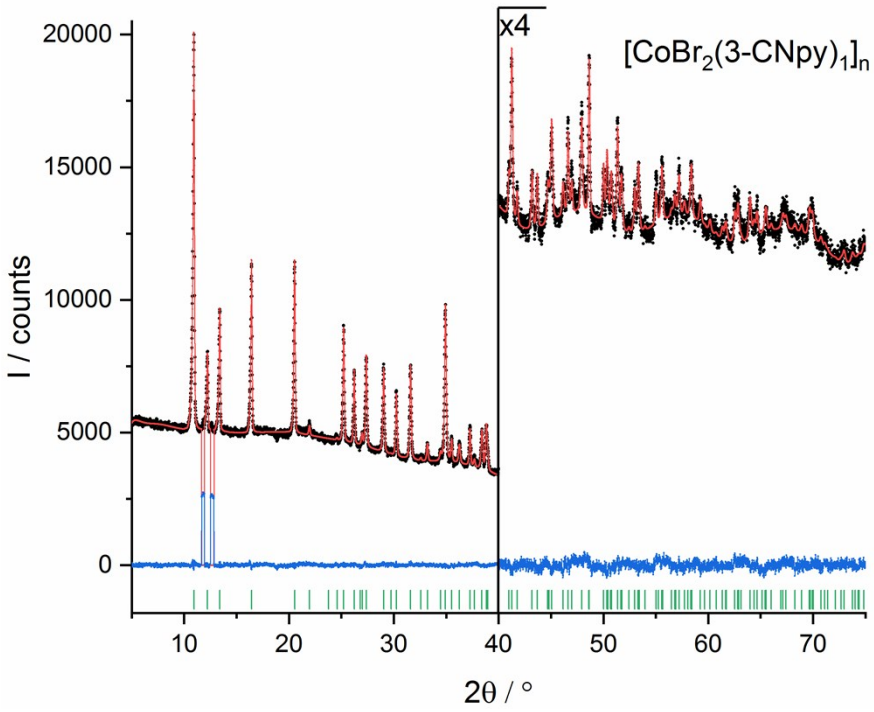

Figure S28. Rietveld plot of **3c**. Observed powder diagram (black points), simulated powder diagram (red solid line), difference profile (blue solid line) and reflection positions (green tick marks). Change of the scale with corresponding factor is indicated in the diagram. Reflections of a foreign phase are excluded.

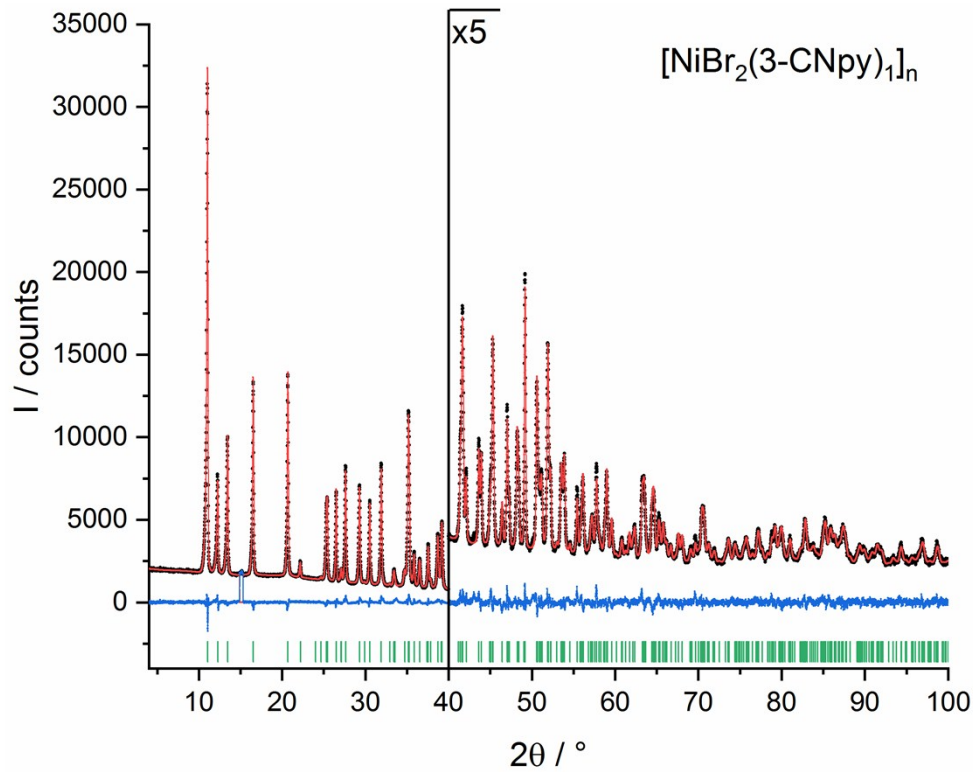

Figure S29. Rietveld plot of **4c**. Observed powder diagram (black points), simulated powder diagram (red solid line), difference profile (blue solid line) and reflection positions (green tick marks). Change of the scale with corresponding factor is indicated in the diagram. An appearing reflection of $NiCl_2$ was excluded.

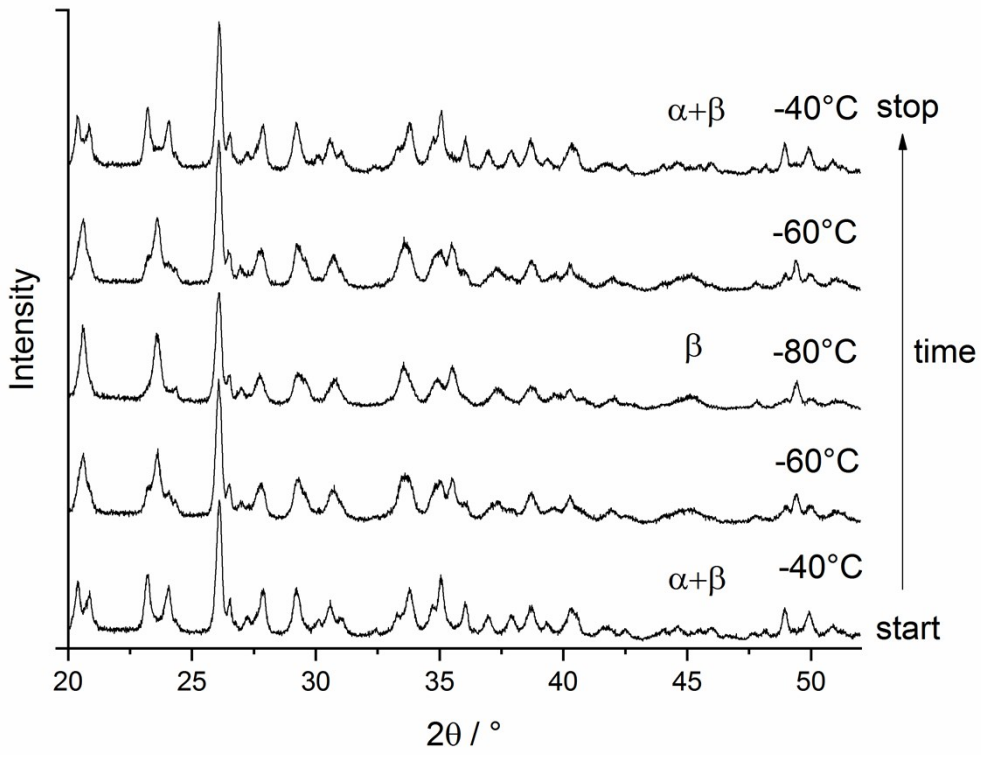

Figure S30. Low-temperature-XRPD series of $[NiBr_2(3\text{-}CNpy)_2]_n$ (**4b**): the phase transition of **β-4b** into **α-4b** is reversible.

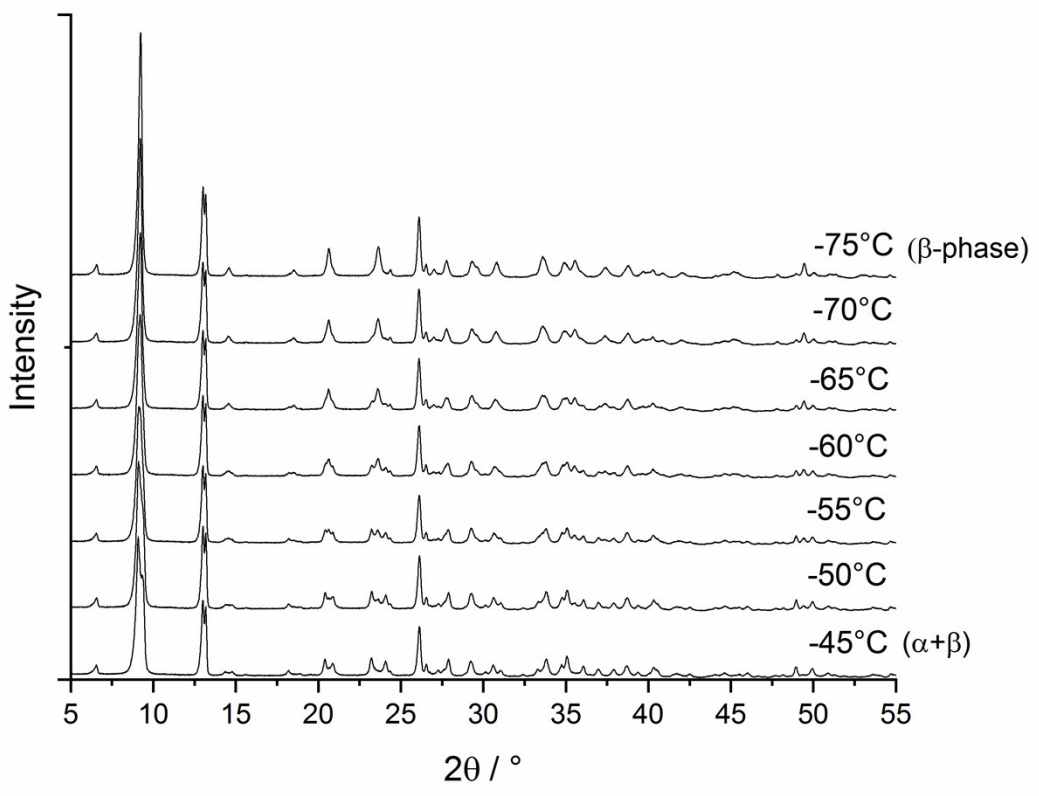

Figure S31. Low-temperature-XRPD series of $[NiBr_2(3\text{-}CNpy)_2]_n$ (**4b**) showing the phase transition in detail. At -75°C the phase transition is completed.

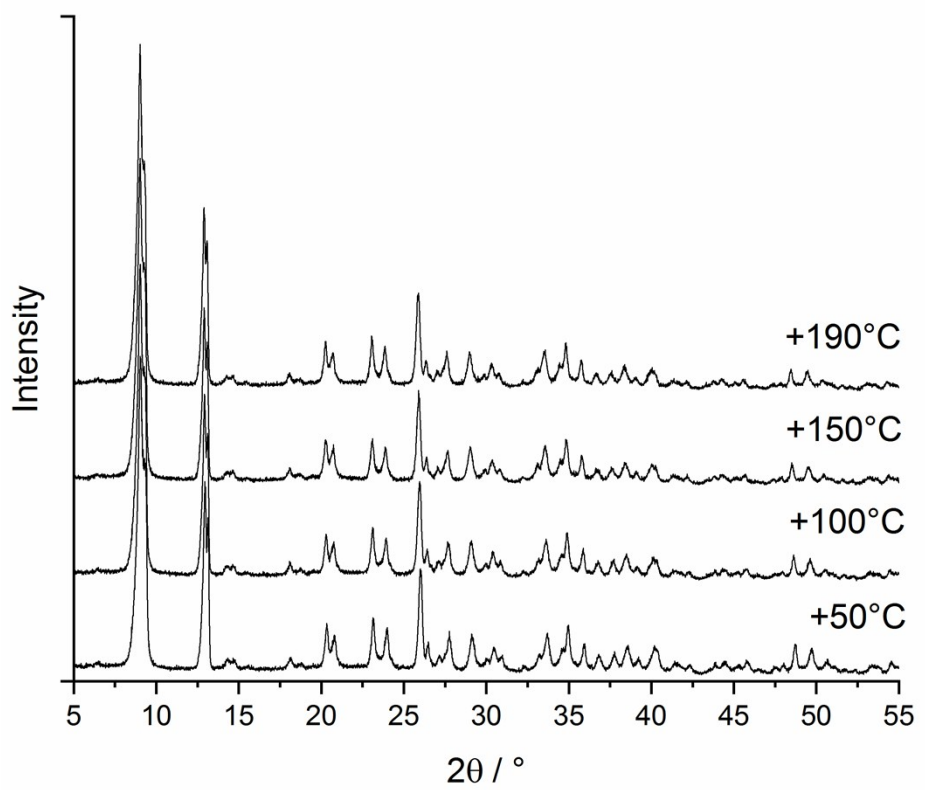

Figure S32. High-temperature-XRPD series of $[NiBr_2(3\text{-}CNpy)_2]_n$ (**4b**): no further phase transition up to 190°C.

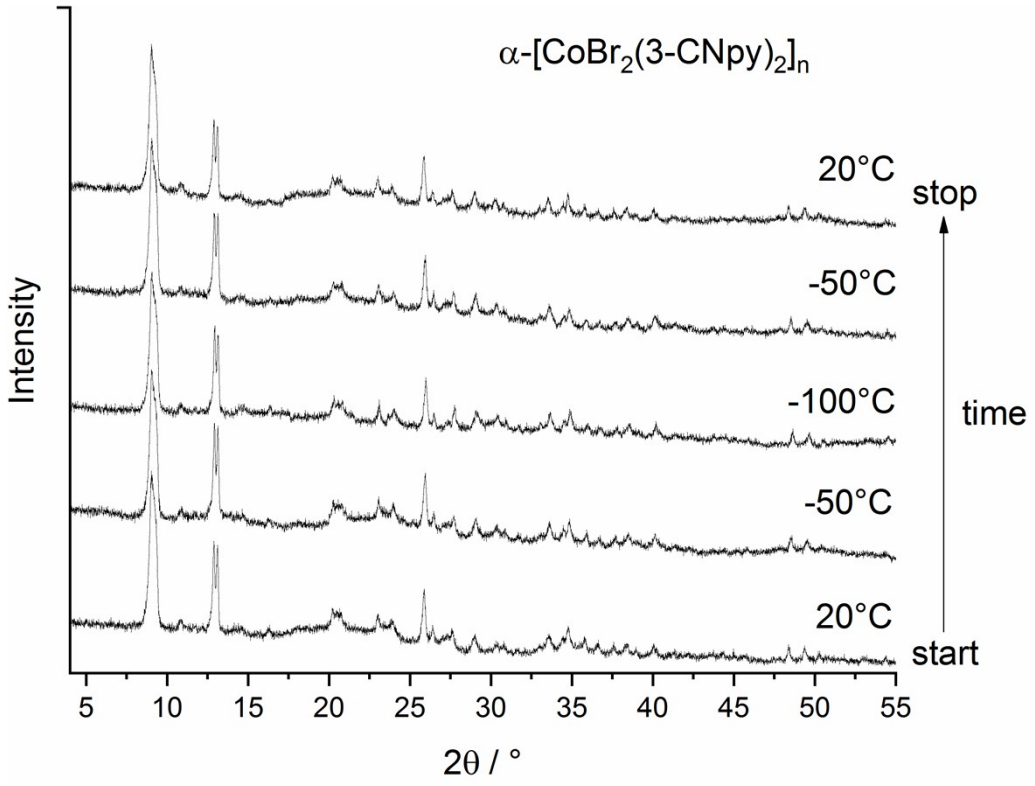

Figure S33. Low-temperature-XRPD series of α-$[CoBr_2(3\text{-}CNpy)_2]_n$ (**α-4b**): no further phase transition down to -100°C.

Table S1. Results of DTA/TG measurements of $[M^{II}Br_2(3\text{-}CNpy)_4]$ (M^{II} = Mn, Fe, Co, Ni). *T*: DTA peak temperatures, m_0: weight of starting compound, Δm_{exp}: relative experimental weight loss, experimental $\Delta m_{exp}/m_0$, calculated $\Delta m_{cal}/m_0$.

Compound	*T* / °C	m_0/ mg	Δm_{exp}/ mg	$\Delta m_{exp}/m_0$ / %	$\Delta m_{cal}/m_0$ / %
$[MnBr_2(3\text{-}CNpy)_4]$		20.72	0	0	0
$[MnBr_2(3\text{-}CNpy)_2]_n$	156.9		6.54	31.54	32.99
$[MnBr_2(3\text{-}CNpy)_1]_n$	244.1		3.32	26.97	24.61
$MnBr_2$	306.4		3.30	30.43	32.66
$[FeBr_2(3\text{-}CNpy)_4]$		21.50	0	0	0
$[FeBr_2(3\text{-}CNpy)_2]_n$	197.4		6.83	31.76	32.94
$[FeBr_2(3\text{-}CNpy)_1]_n$	245.8		3.35	22.82	24.56
$FeBr_2$	318		2.79	24.56	32.55
$[CoBr_2(3\text{-}CNpy)_4]$		20.72	0	0	0
$[CoBr_2(3\text{-}CNpy)_2]_n$	198.8		6.61	31.90	32.78
$[CoBr_2(3\text{-}CNpy)_1]_n$	250.3		3.25	23.05	24.37
$CoBr_2$	313.63		2.37	21.90	32.24
$[NiBr_2(3\text{-}CNpy)_4]$		26.43	0	0	0
$[NiBr_2(3\text{-}CNpy)_2]_n$	217.8		8.32	31.52	32.77
$[NiBr_2(3\text{-}CNpy)_1]_n$	281.2		4.04	22.33	24.37
$NiBr_2$	346.8		3.92	27.88	32.22

Table S2. Crystallographic data of $[M^{II}Br_2(3\text{-}CNpy)_4]$.

	1a	**2a**	**3a**	**4a**
Compound	$[MnBr_2(3\text{-}CNpy)_4]$	$[FeBr_2(3\text{-}CNpy)_4]$	$[CoBr_2(3\text{-}CNpy)_4]$	$[NiBr_2(3\text{-}CNpy)_4]$
CSD number	1845140	1845149	1845152	1845162
Formula	$C_{24}H_{16}Br_2MnN_8$	$C_{24}H_{16}Br_2FeN_8$	$C_{24}H_{16}Br_2CoN_8$	$C_{24}H_{16}Br_2NiN_8$
Crystal system	Tetragonal	Tetragonal	Tetragonal	Tetragonal
Space group (No.)	*P* 4*nc* (104)	*P* 4*nc* (104)	*P* 4*nc* (104)	*P* 4*nc* (104)
MW /g·mol^{-1}	631.19	632.10	635.20	634.94
***a* /Å**	11.2178(5)	11.1484(2)	11.0587(4)	10.9722(9)
***c* /Å**	10.3309(6)	10.3205(2)	10.4149(5)	10.4600(3)
***V* /Å^3**	1300.0(3)	1282.7(1)	1273.7(1)	1259.3(2)
Z, Z'	2, 1/4	2, 1/4	2, 1/4	2, 1/4
Site symmetry of M^{II}	4	4	4	4
D_{calc} /Mg·m^{-3}	1.612	1.637	1.656	1.674
T /K	298	298	298	298
Radiation type	Cu $K\alpha_1$	Cu $K\alpha_1$	Cu $K\alpha_1$	Cu $K\alpha_1$
Wavelength /Å	1.54056	1.54056	1.54056	1.54056
$2\Theta_{max}$ /°	100	95	100	100
R_p /%	1.587	1.821	1.039	4.179
R_{wp} /%	2.038	2.315	1.335	5.366
R_{exp} /%	1.959	2.279	1.150	2.891
GOF	1.042	1.015	1.162	1.856
R_p' /% [a]	11.095	16.854	18.098	8.492
R_{wp}' /% [a]	8.292	10.980	12.177	9.616
R_{exp}' /% [a]	7.971	10.812	10.484	5.181
(a) *R*', R_{wp}' and R_p' values are background corrected according to the reference [41].				

Table S3. Crystallographic data of $[M^{II}Br_2(3\text{-}CNpy)_2]_n$.

	1b	**2b**	**α-3b**	**β-3b**	**α-4b**	**β-4b**
Compound	$[MnBr_2(3\text{-}CNpy)_2]_n$	$[FeBr_2(3\text{-}CNpy)_2]_n$	$[CoBr_2(3\text{-}CNpy)_2]_n$	$[CoBr_2(3\text{-}CNpy)_2]_n$	$[NiBr_2(3\text{-}CNpy)_2]_n$	$[NiBr_2(3\text{-}CNpy)_2]_n$
CSD number	1845141	1845150	1845157	1845160	1845163	1845164
Formula	$C_{12}H_8Br_2MnN_4$	$C_{12}H_8Br_2FeN_4$	$C_{12}H_8Br_2CoN_4$	$C_{12}H_8Br_2CoN_4$	$C_{12}H_8Br_2NiN_4$	$C_{12}H_8Br_2NiN_4$
MW /g·mol^{-1}	422,96	423,87	426,95	426,95	426,71	426,71
Crystal system	Orthorhombic	Orthorhombic	Orthorhombic	Triclinic	Monoclinic	Triclinic
Space group (No.)	*P n n m* (58)	*P n n m* (58)	*P n n m* (58)	$P\bar{1}$ (2)	*C c* (9)	$P\bar{1}$ (2)
***a* /Å**	27.304(6)	27.128(5)	27.019(1)	3.727(5)	3.709(1)	3.727(4)
***b* /Å**	7.221(9)	7.172(2)	7.124(2)	13.629(6)	26.801(4)	13.574(9)
***c* /Å**	3.829(7)	3.788(1)	3.759(7)	13.868(6)	13.706(8)	13.761(6)
***α* /°**	90	90	90	87.37(7)	90	86.86(2)
***ß* /°**	90	90	90	82.34(4)	97.67(8)	82.40(1)
***γ* /°**	90	90	90	82.40(5)	90	82.12(1)
***V* /Å^3**	755.1(8)	737.0(2)	723.7(1)	697.2(2)	1350.5(8)	683.1(5)
Z, Z'	2, 1/4	2, 1/4	2, 1/4	2, 1	4, 1	2, 1
Site symmetry of M^{II}	2/*m*	2/*m*	2/*m*	$\bar{1}$, $\bar{1}$	1	$\bar{1}$, $\bar{1}$
***D*$_{calc}$ /Mg·m^{-3}**	1.860	1.910	1.959	2.034	2.099	2.075
T /K	298	298	298	298	125	298
Radiation type	Cu $K\alpha_1$	Cu $K\alpha_1$	Cu $K\alpha_1$	Cu $K\alpha_1$	Cu $K\alpha_1$	Cu $K\alpha_1$
Wavelength /Å	1.54056	1.54056	1.54056	1.54056	1.54056	1.54056
2Θ$_{max}$ /°	100	95	85 [a]	85 [a]	90	70
***R$_p$* /%**	2.095	1.315	1.388 [a]	1.388 [a]	3.547	3.277 [b]
***R$_{wp}$* /%**	2.694	1.674	1.823 [a]	1.823 [a]	5.026	4.294 [b]
***R$_{exp}$* /%**	2.231	1.484	1.286 [a]	1.286 [a]	2.753	2.473 [b]
GOF	1.208	1.127	1.417 [a]	1.417 [a]	1.825	1.737 [b]
***R$_p$'* /%** [c]	12.388	16.206	20.614 [a]	20.614 [a]	6.262	5.999 [b]
***R$_{wp}$'* /%** [c]	10.234	11.332	15.842 [a]	15.842 [a]	5.026	7.376 [b]
***R$_{exp}$'* /%** [c]	8.474	10.052	11.182 [a]	11.182 [a]	4.568	4.294 [b]
Pyridine stacking angle /° [d]	90	90	90	88.9(8)	86.7(3)	88.8(2)

(a) Rietveld refinement of a sample containing a mixture of α-phase (59.4%) and β-phase (41.6%).
(b) Rietveld refinement of a sample containing a mixture of α-phase (18.7%) and β-phase (81.3%).
(c) *R'*, *R$_{wp}$'* and *R$_p$'* values are background corrected according to the reference [41].
(d) Angle between the pyridine ring mean plane and the stacking direction
(for **1b** - **α-3b**: [001] and for **β-3b** - **β-4b** [100].)

Table S4. Crystallographic data of $[M^{II}Br_2(3\text{-}CNpy)_1]_n$.

	1c	**2c**	**3c**	**4c**
Compound	$[MnBr_2(3\text{-}CNpy)_1]_n$	$[FeBr_2(3\text{-}CNpy)_1]_n$	$[CoBr_2(3\text{-}CNpy)_1]_n$	$[NiBr_2(3\text{-}CNpy)_1]_n$
CSD number	1845142	1845151	1845161	1845165
Formula	$C_6H_4Br_2MnN_2$	$C_6H_4Br_2FeN_2$	$C_6H_4Br_2CoN_2$	$C_6H_4Br_2NiN_2$
MW /g·mol^{-1}	318.86	319.76	322.85	322.61
Crystal system	Monoclinic	Orthorhombic	Orthorhombic	Orthorhombic
Space group (No.)	*P* 1 1 2_1 [a] (4)	*P m c* 2_1 (26)	*P m c* 2_1 (26)	*P m c* 2_1 (26)
***a* /Å**	3.834(7)	3.772(2)	3.740(1)	3.701(5)
***b* /Å**	7.258(1)	7.251(2)	7.231(2)	7.204(8)
***c* /Å**	16.547(7)	16.31(1)	16.167(6)	16.000(4)
***α* /°**	90	90	90	90
***ß* /°**	90	90	90	90
***γ* /°**	93.41(1)	90	90	90
***V* /Å^3**	459.7(5)	446.1(8)	437.2(1)	426.7(1)
Z, Z'	2, 1	2, 1/2	2, 1/2	2, 1/2
Site symmetry of M	1	*m*	*m*	*m*
***D*$_{calc}$ /Mg·m^{-3}**	2.303	2.381	2.452	2.511
T /K	298	298	298	125
Radiation type	Cu *Kα*$_1$	Cu *Kα*$_1$	Cu *Kα*$_1$	Cu *Kα*$_1$
Wavelength /Å	1.54056	1.54056	1.54056	1.54056
2Θ$_{max}$ /°	80	100	100	100
***R*$_p$ /%**	1.696	1.633	1.506	2.715
***R*$_{wp}$ /%**	2.147	2.077	1.912	3.520
***R*$_{exp}$ /%**	1.695	1.714	1.555	2.757
GOF	1.266	1.212	1.230	1.277
***R*$_p$' /%** [b]	14.577	18.079	21.223	7.416
***R*$_{wp}$' /%** [b]	12.191	12.838	14.320	7.626
***R*$_{exp}$' /%** [b]	9.630	10.594	11.642	5.973

(a) For ease of comparison of 1c to 4c a non-standard space-group setting was used for 1c. *P* 112_1 is a non-standard setting of *P* 2_1.
(b) *R'*, R_{wp}' and R_p' values are background corrected according to the reference [41].

Text S1

Details on syntheses of $[M^{II}Br_2(3\text{-}CNpy)_4]$

Synthesis of $[MnBr_2(3\text{-}CNpy)_4]$ (1a). $MnBr_2$ (0.5g, 2.33mmol) was dissolved in 15mL ethanol, 3-cyanopyridine (0.96g, 9.22mmol) was dissolved in 35mL ethanol. By mixing both solutions, a colorless powder was obtained. IR (cm^{-1}): 3091(w), 2241(m) 1595(s); 1470(s), 1418(s), 1039(s), 1032(s), 818(s), 691(s), 644(s).

Synthesis of $[FeBr_2(3\text{-}CNpy)_4]$ (2a). $FeBr_2$ (0.2g, 0.93mmol) was dissolved in 15mL ethanol, 3-cyanopyridine (0.96g, 9.22mmol) was dissolved in 35mL ethanol. By mixing both solutions, a yellow powder was obtained. IR (cm^{-1}): 3092(w), 2241(m), 1595(s), 1468(s), 1418(s), 1042(m), 1034(m), 816(s), 691(s), 644(s).

Synthesis of $[CoBr_2(3\text{-}CNpy)_4]$ (3a). $CoBr_2$ (0.5g, 2.286mmol) was dissolved in 30mL methanol, 3-cyanopyridine (1g, 9.605mmol) was dissolved in 35mL methanol. By mixing both solutions, a violett powder was obtained. IR(cm^{-1}): 3102(w), 2241(m), 1597(s), 1470(m), 1418(m), 1042(m), 1034(m), 816(s), 692(s), 646(s).

Synthesis of $[NiBr_2(3\text{-}CNpy)_4]$ (4a). $NiBr_2$ (0.202 g, 0.924mmol) was dissolved in 30mL DAA, 3-cyanopyridine (0.4g, 3.839mmol) was dissolved in 35 mL DAA. By mixing both solutions, a light green powder was obtained. IR (cm^{-1}): 3103 (w), 2243(s) 1597(s); 1470(s), 1410(s), 1044(m), 1034(m), 816(s), 692(s), 648(m).

Text S2

Details on preparation of $[M^{II}Br_2(3\text{-}CNpy)_2]_n$

Preparation of $[MnBr_2(3\text{-}CNpy)_2]_n$ (1b). 1b was prepared by thermal decomposition of $[MnBr_2(3cypy)_4]$ (**1a**). A flesh-colored powder was obtained. IR (cm^{-1}): 3086(w), 2239(m), 1597(m), 1474(m), 1418(s), 1059(m), 1042(m), 800(s), 687(s), 648(s).

Preparation of $[FeBr_2(3\text{-}CNpy)_2]_n$ (2b). 2b was prepared by thermal decomposition of $[FeBr_2(3cypy)_4]$ (**2a**). A red powder was obtained and immediately transferred into a glass capillary (diameter: 0.5mm) that was sealed afterwards. IR (cm^{-1}): 3084(w), 2240(m), 1597(m), 1474(m), 1418(s), 1042(m), 799(s), 685(s), 650(s).

Preparation of $[CoBr_2(3\text{-}CNpy)_2]_n$ (3b). 3b was prepared by thermal decomposition of $[CoBr_2(3cypy)_4]$ (**3a**). A lilac powder was obtained. XRPD data revealed that this procedure generally leads to a mixture of **α-3b** and **β-3b**. A phase-pure sample of **α-3b** could not be obtained. Only once **β-3b** as pure phase could be obtained. IR(cm^{-1}) of the mixture: 3102(w), 2236(m), 1599(s), 1472(m), 1419(s), 1045(m), 810(s), 797(s) 685(s), 650(s).

Preparation of $[NiBr_2(3\text{-}CNpy)_2]_n$ (4b). α-4b and **β-4b** were prepared by thermal decomposition of $[NiBr_2(3cypy)_4]$ (**4a**). XRPD data revealed that this procedure generally leads to a mixture of **β-4b** with a slight amount of **α-4b**. **α-4b** as pure phase can be obtained by cooling the mixture to -100°C. Pure **β-4b** could not be obtained. IR(cm^{-1}) of the mixture: 3071(w), 2236(s), 1601(s), 1474(m), 1423(m), 1047(w), 1036(m) 808(s), 687(s).

Text S3

Details on preparation of $[M^{II}Br_2(3\text{-}CNpy)_1]_n$

Preparation of $[MnBr_2(3\text{-}CNpy)_1]_n$ (1c). 1c was prepared by thermal decomposition of $[MnBr_2(3cypy)_2]_n$ (**1b**). A light grey powder was obtained. IR (cm^{-1}): 3059(w), 2272(s), 1597(m), 1474(m), 1418(s), 1059(m), 1043(m), 800(s), 687(s), 648(s).

Preparation of $[FeBr_2(3\text{-}CNpy)_1]_n$ (2c). 2c was prepared by thermal decomposition of $[FeBr_2(3cypy)_2]_n$ (**2b**). An ochre powder was obtained. IR (cm^{-1}): 3061(w), 2278(s), 1680(s), 1595(m), 1541(m), 1460(m), 1417(s), 1049(m), 1034(m), 806(s), 682(w), 667(m).

Preparation of $[CoBr_2(3\text{-}CNpy)_1]_n$ (3c). 3c was prepared by thermal decomposition of $[CoBr_2(3cypy)_2]_n$ (**3b**). A light lilac powder was obtained. IR(cm^{-1}): 3102(w), 2287(m), 1622(s), 1603(s), 1573(w), 1481(m), 1422(s), 808(s), 687(m), 652(s).

Preparation of $[NiBr_2(3\text{-}CNpy)_1]_n$ (4c) was prepared by thermal decomposition of $[FeBr_2(3cypy)_4]$ (**4a**). A greyish ochre powder was obtained. IR(cm^{-1}): 3057(m), 2288(s), 1599(s), 1477(m), 1418(s), 1034(m) 797(s), 683(s), 654(m).

Text S4

Details on structure solutions

$[FeBr_2(3\text{-}CNpy)_1]_n$ (2c). The structure of **4c** was used as starting point for the Rietveld refinement. Reflections of an unknown foreign phase were excluded during Pawley and Rietveld refinement (2θ range from 11.51° to 11.85°, 12.40° to 12.71°, 24.30° to 24.54°).

$[CoBr_2(3\text{-}CNpy)_2]_n$ (α-3b/ β-3b). XRPD data were collected at room temperature**.** For **α-3b** 20 reflections in the low angle range were carefully selected for indexing, which led in an orthorhombic unit cell with Z = 2 and lattice parameters similar to those of compounds **1b** and **2b**. In the first Rietveld refinement reflections of **β-3b** were excluded. For the subsequent simultaneous refinement of both phases, the structure of **β-4b** was used as starting point for **β-3b**. The investigated sample contained 59.4% of **α-3b** and 41.6% of **β-3b**. The final crystallographic data of both phases were taken from the simultaneous refinement.

$[CoBr_2(3\text{-}CNpy)_1]_n$ (3c). The structure of **4c** was used as starting point for the Rietveld refinement. Reflections of an unknown foreign phase were excluded during Pawley and Rietveld refinement (2θ range from 11.675° to 11.93°, 12.52° to 12.83°).

$[NiBr_2(3\text{-}CNpy)_2]_n$ (α-4b). XRPD data of a phase-pure sample were collected at -150°C.

$[NiBr_2(3\text{-}CNpy)_2]_n$ (β-4b). The structure of **α-4b** was used as a starting point for the structure solution of **β-4b**. The structure was solved by a fit to the room-temperature powder diagram (measured at room temperature) of the β-phase using the program FIDEL “Fit with deviating lattice parameters” [43], which uses a similarity index based on cross-correlation functions. Details will be published elsewhere [44]. The final Rietveld refinement revealed that the investigated sample contained 18.7% of the α-phase and 81.3% of the β-phase.